Supplement of Biogeosciences, 22, 6669–6693, 2025 https://doi.org/10.5194/bg-22-6669-2025-supplement © Author(s) 2025. CC BY 4.0 License.





Supplement of

Aerodynamic flux-gradient measurements of ammonia over four spring seasons in grazed grassland: environmental drivers, methodological challenges and uncertainties

Mubaraq Olarewaju Abdulwahab et al.

Correspondence to: Christophe Flechard (christophe.flechard@inrae.fr)

The copyright of individual parts of the supplement might differ from the article licence.

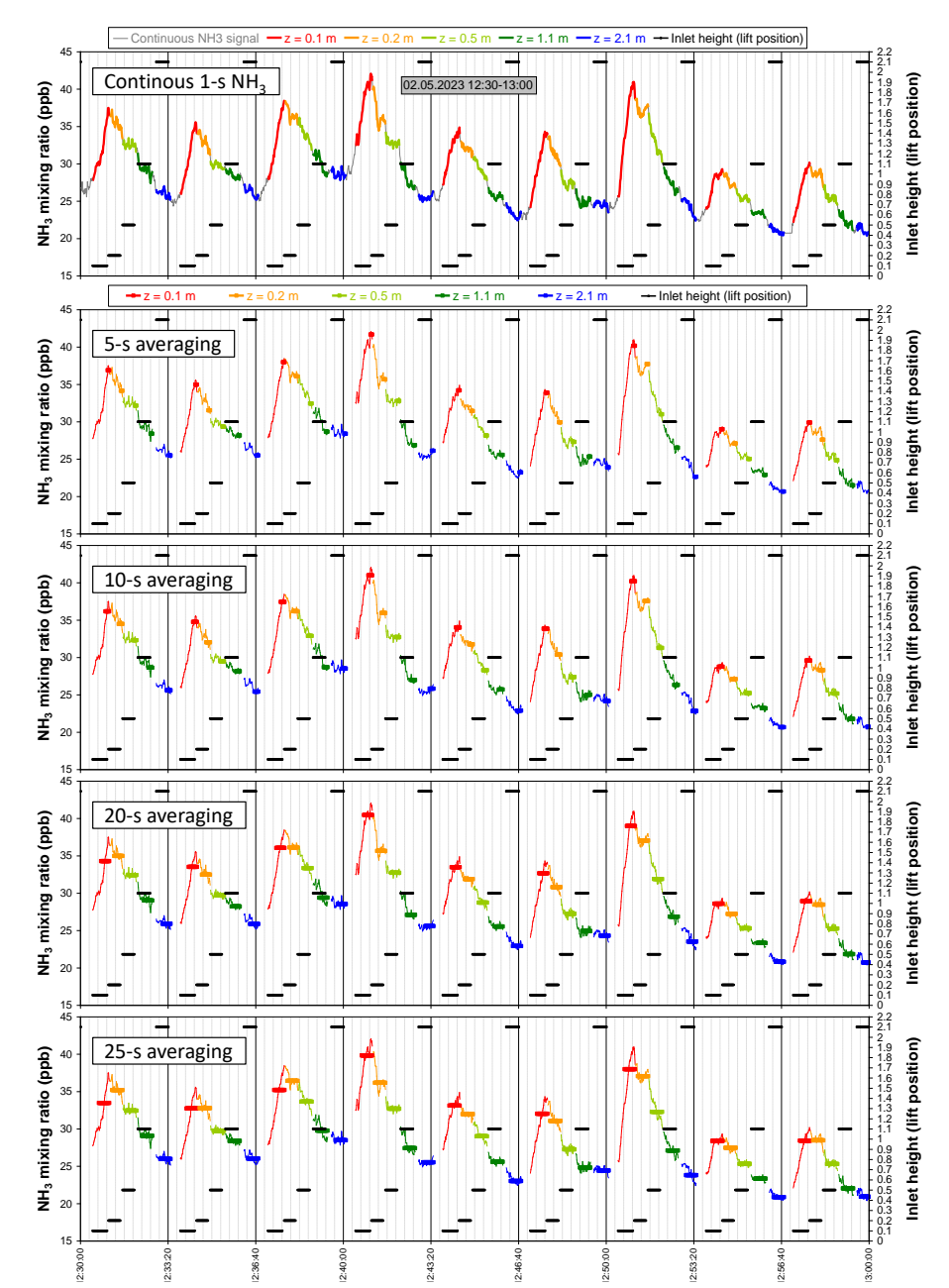


Figure S1: An example half-hour of high frequency (1-sec) gradient-lift data, showing nine consecutive mast ascents by the lift carrying the air inlet. The top panel shows the 1-sec continuous NH₃ time series, with concentrations measured at different heights when the inlet was stationary (colors red to blue) or moving between heights (grey line). All fluxes in the main paper were calculated using a 10-sec averaging time (5 seconds before + 5 seconds after end of a given position); other averaging times from 5 to 25 seconds are shown for comparison. The data show the need for sufficient equilibration time between heights in order to minimize carry-over effects, which inevitably reduce the magnitude of the gradient. The effect was naturally strongest for the lift descent from top (2.1 m) to bottom (0.1m); however, this did not affect flux calculations very strongly (see Fig. S2) since the lower two heights (0.1 and 0.2m) were not used in gradient calculations.

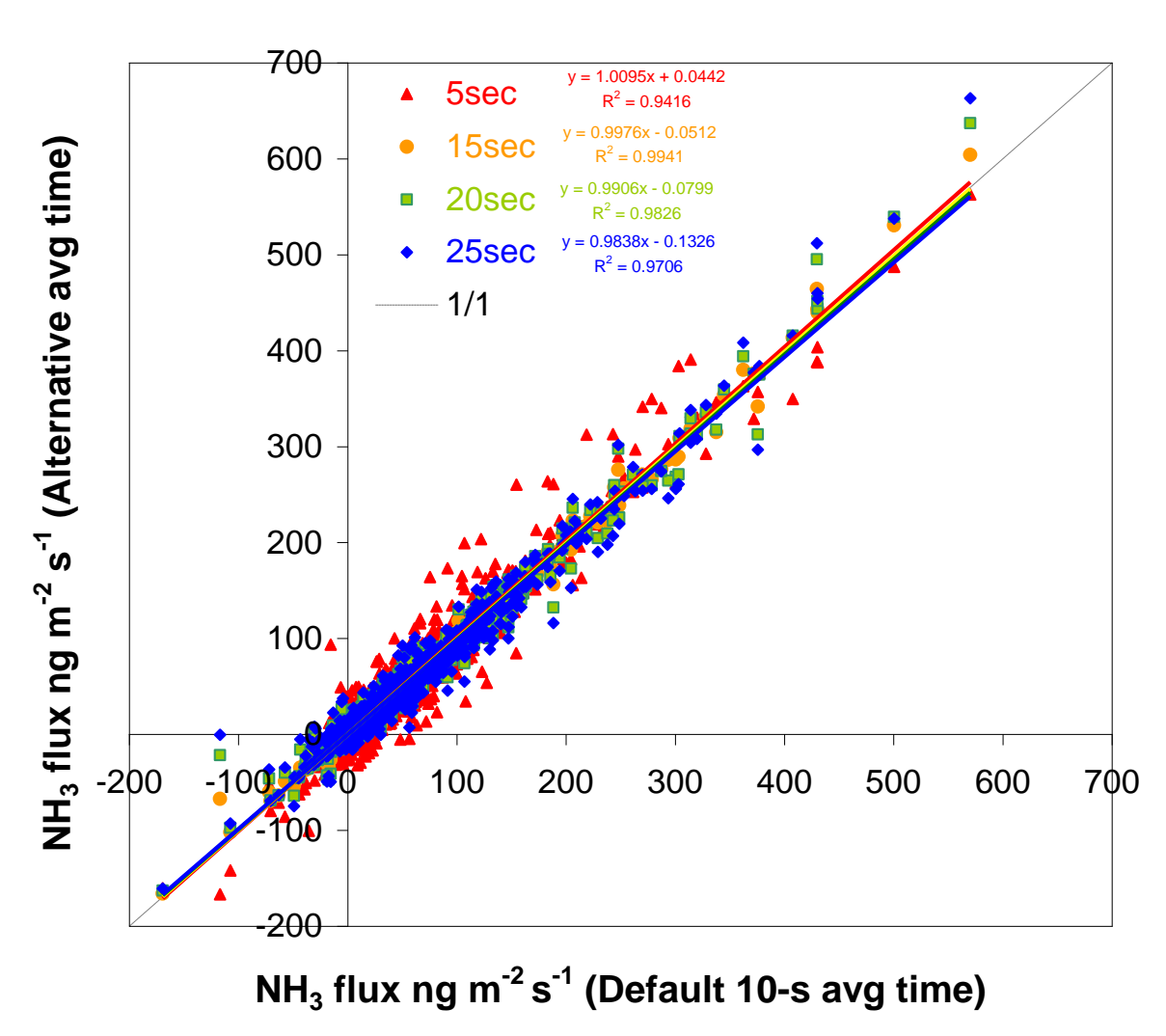
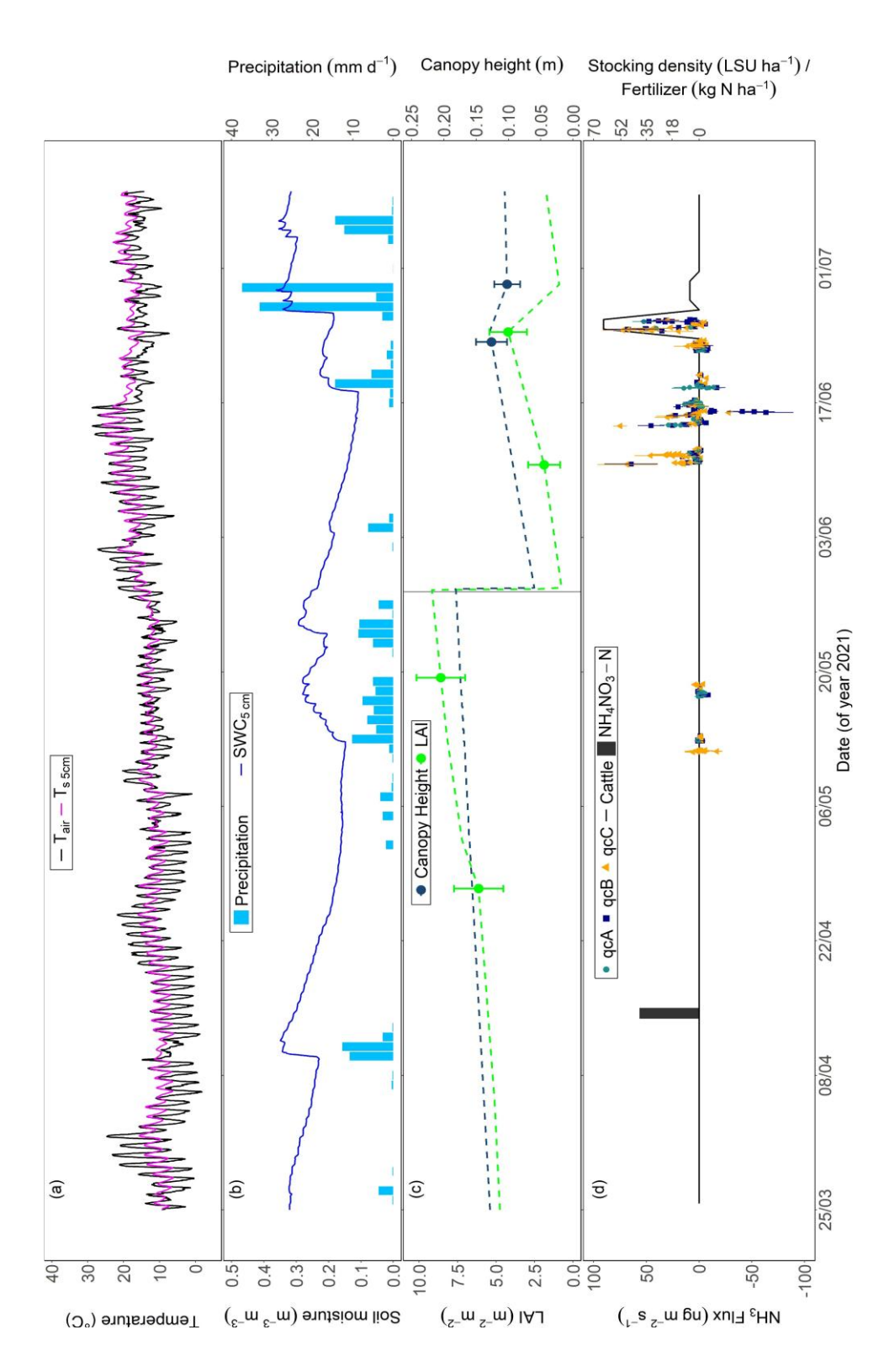
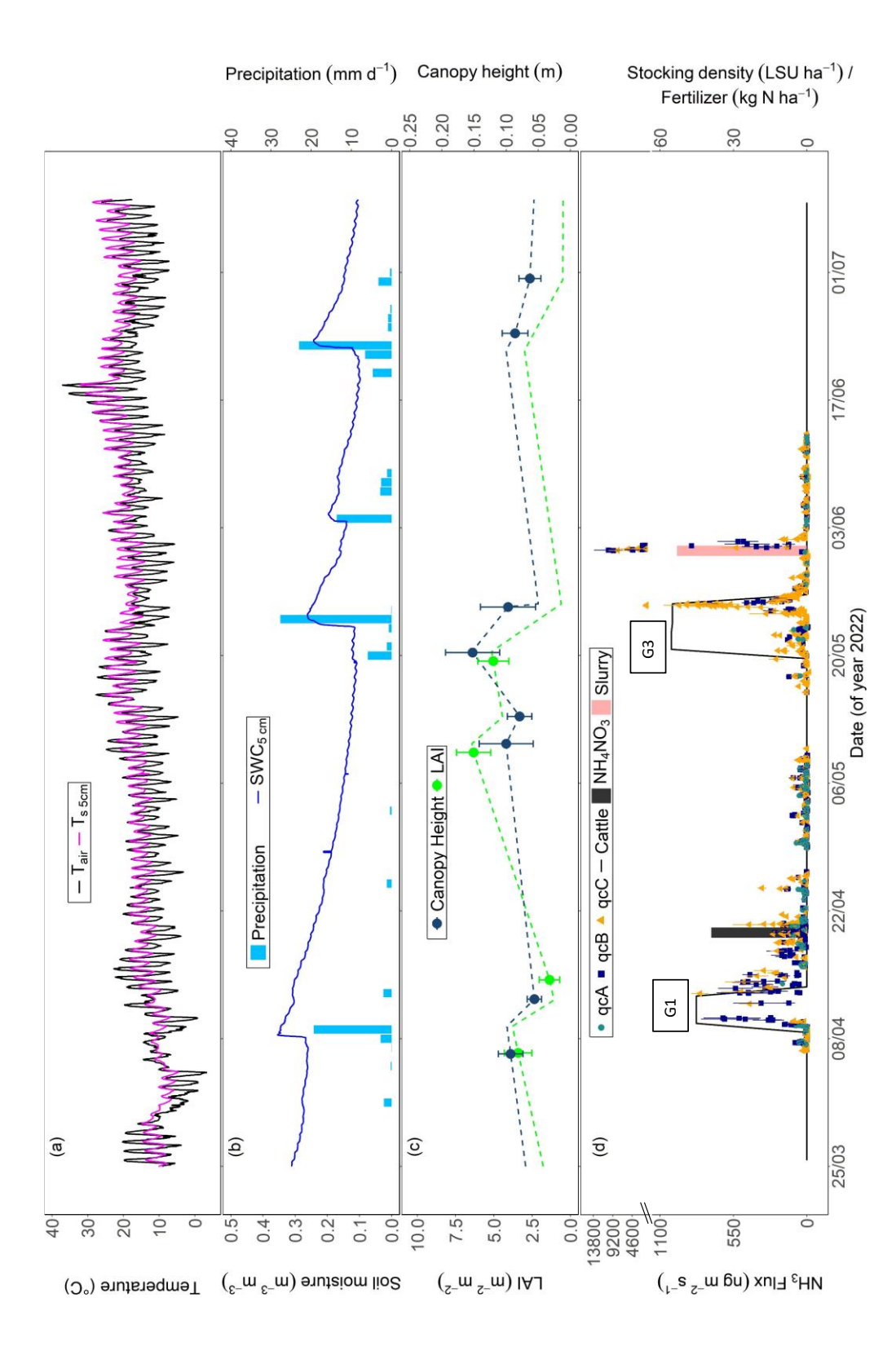


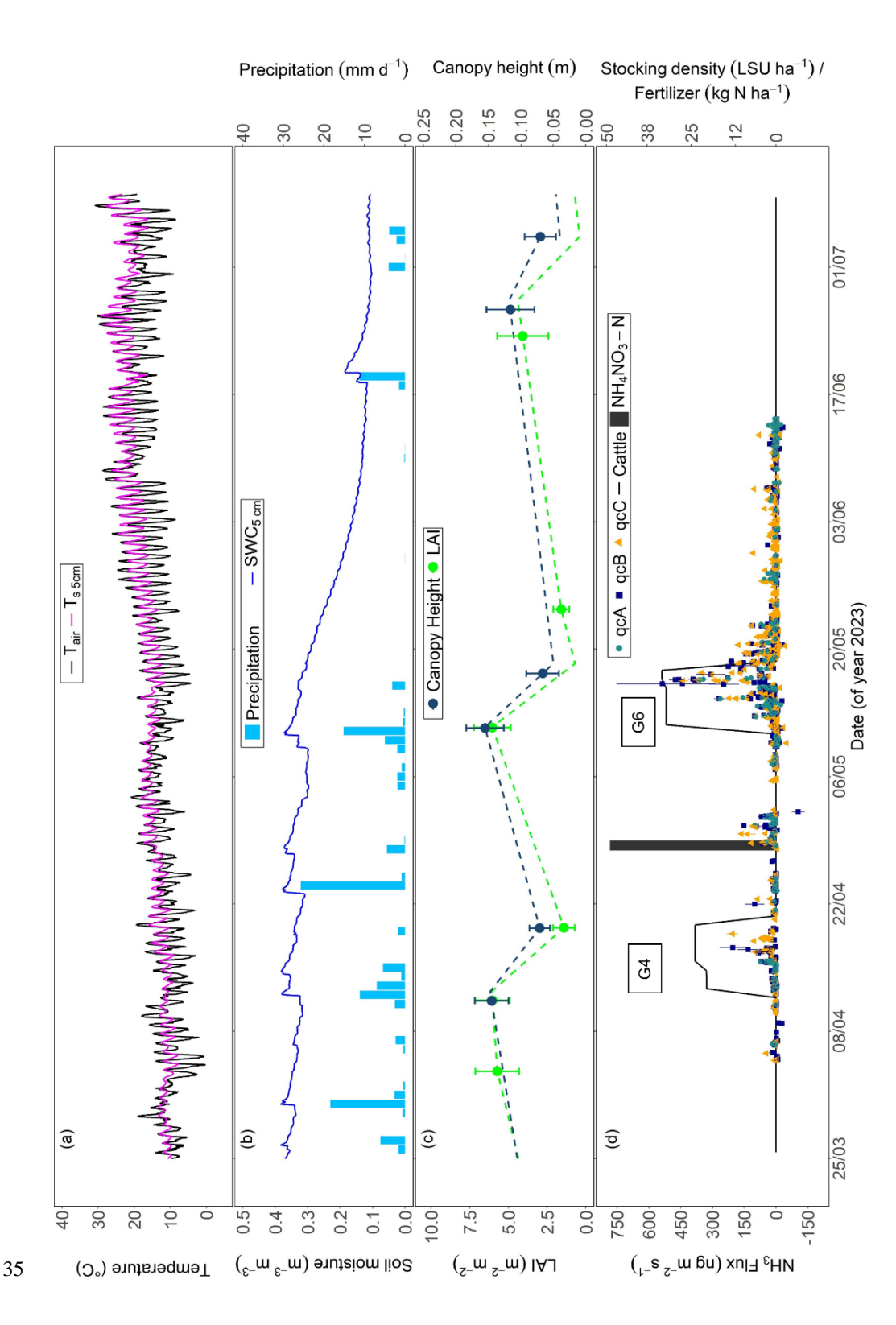
Figure S2: Sensitivity test of calculated fluxes (for 2023 data) to the averaging time chosen for high-frequency NH₃ concentrations at the end of each sampling height, following the scheme shown in Fig. S1, with 10-seconds being the averaging time used in all flux calculations shown in the main article. The calculated fluxes are not very sensitive to the averaging time (all slopes near 1 and offsets near 0). This is primarily because the 0.1 and 0.2m heights were excluded from the gradient calculations (see main article), while the longer equilibration time required was for the lift descent from the top (2.1 m) to the bottom (0.1 m) heights, as shown in Fig. S1.



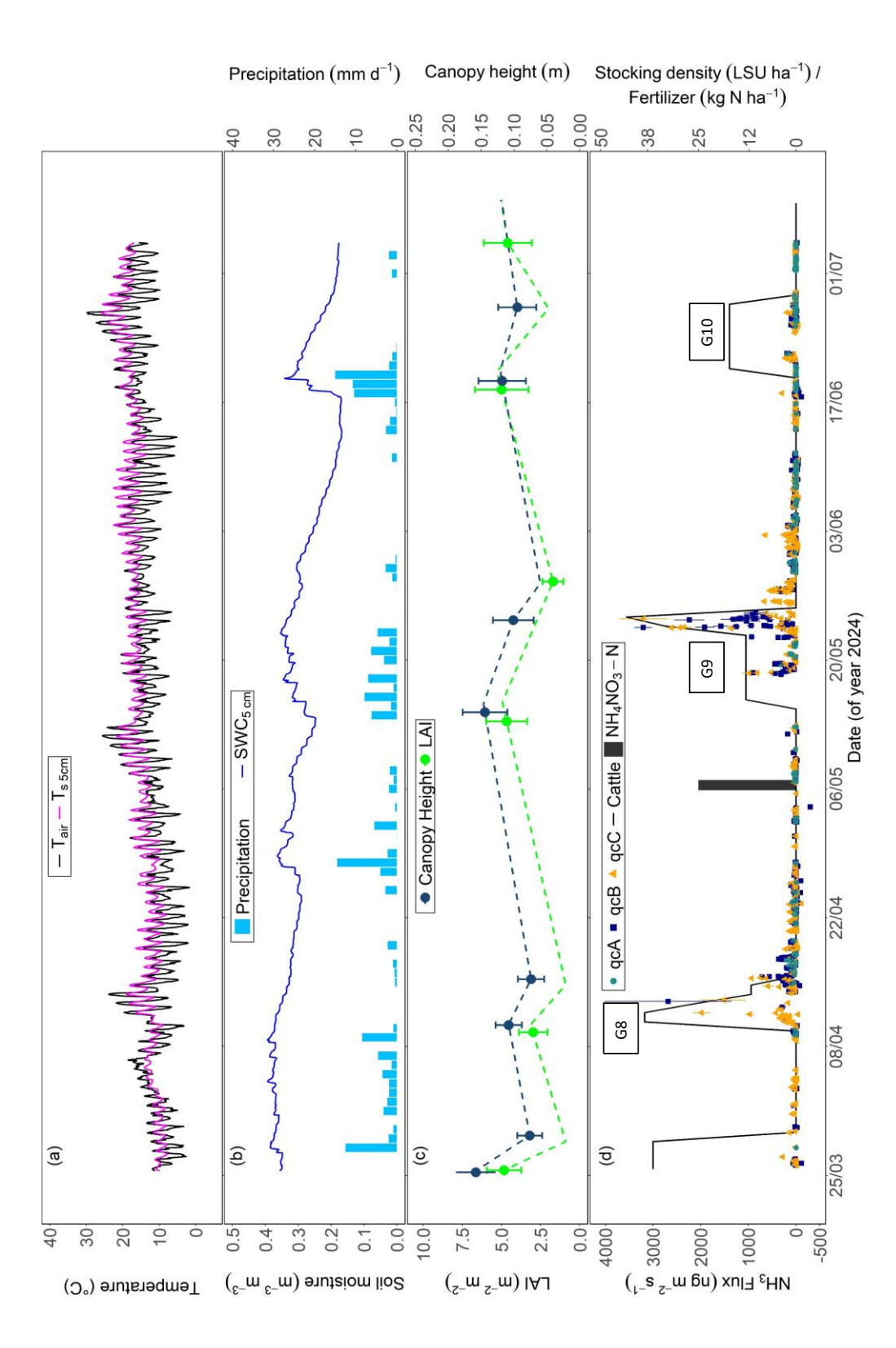
and canopy height. (d) NH3 fluxes are categorized by quality classes (qcA, qcB and qcC, as defined in the main text), alongside Figure S3: Time series of measured NH3 fluxes, environmental conditions, and management events during spring 2021 for plot A. (a) Air temperature and soil temperature at 5 cm depth. (b) Precipitation and soil moisture at 5 cm depth. (c) Leaf area index (LAI) stocking density (black line) and fertilizer application (black bars). Grass cuts are shown only for 2021, as no cutting occurred in subsequent years.



and canopy height. (d) NH3 fluxes are categorized by quality classes (qcA, qcB and qcC, as defined in the main text), alongside (a) Air temperature and soil temperature at 5 cm depth. (b) Precipitation and soil moisture at 5 cm depth. (c) Leaf area index (LAI) Figure S4: Time series of measured NH3 fluxes, environmental conditions, and management events during spring 2022 for plot A. stocking density (black line) and fertilizer application (black and pink bars).



(a) Air temperature and soil temperature at 5 cm depth. (b) Precipitation and soil moisture at 5 cm depth. (c) Leaf area index (LAI) and canopy height. (d) NH3 fluxes are categorized by quality classes (qcA, qcB and qcC, as defined in the main text), alongside Figure S5: Time series of measured NH3 fluxes, environmental conditions, and management events during spring 2023 for plot A. stocking density (black line) and fertilizer application (black and pink bars).



Air temperature and soil temperature at 5 cm depth. (b) Precipitation and soil moisture at 5 cm depth. (c) Leaf area index (LAI) and canopy height. (d) NH3 fluxes are categorized by quality classes (qcA, qcB and qcC, as defined in the main text), alongside stocking density (black line) and fertilizer application (black bars). Figure S6: Time series of measured NH3 fluxes, environmental conditions, and management events during spring 2024 for plot A. (a)

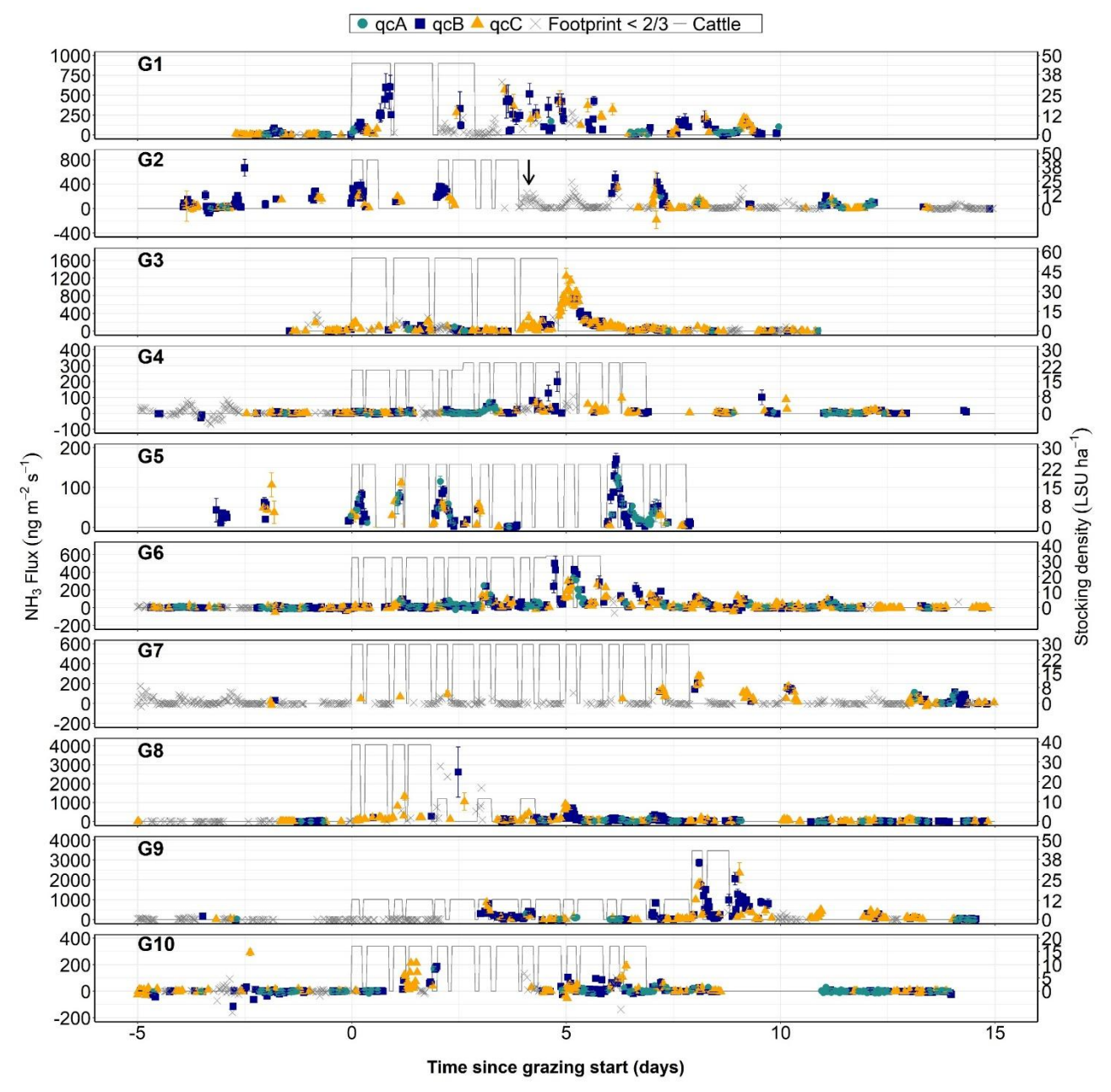


Figure S7: Similar to Fig. 4 of the main article, but showing valid NH₃ fluxes without footprint correction, and indicating in addition (grey crosses) fluxes that were micrometeorologically valid but for which the required footprint criteria (> 2/3) were not satisfied. The latter were almost systematically significantly lower than the former, highlighting the importance of footprint correction.

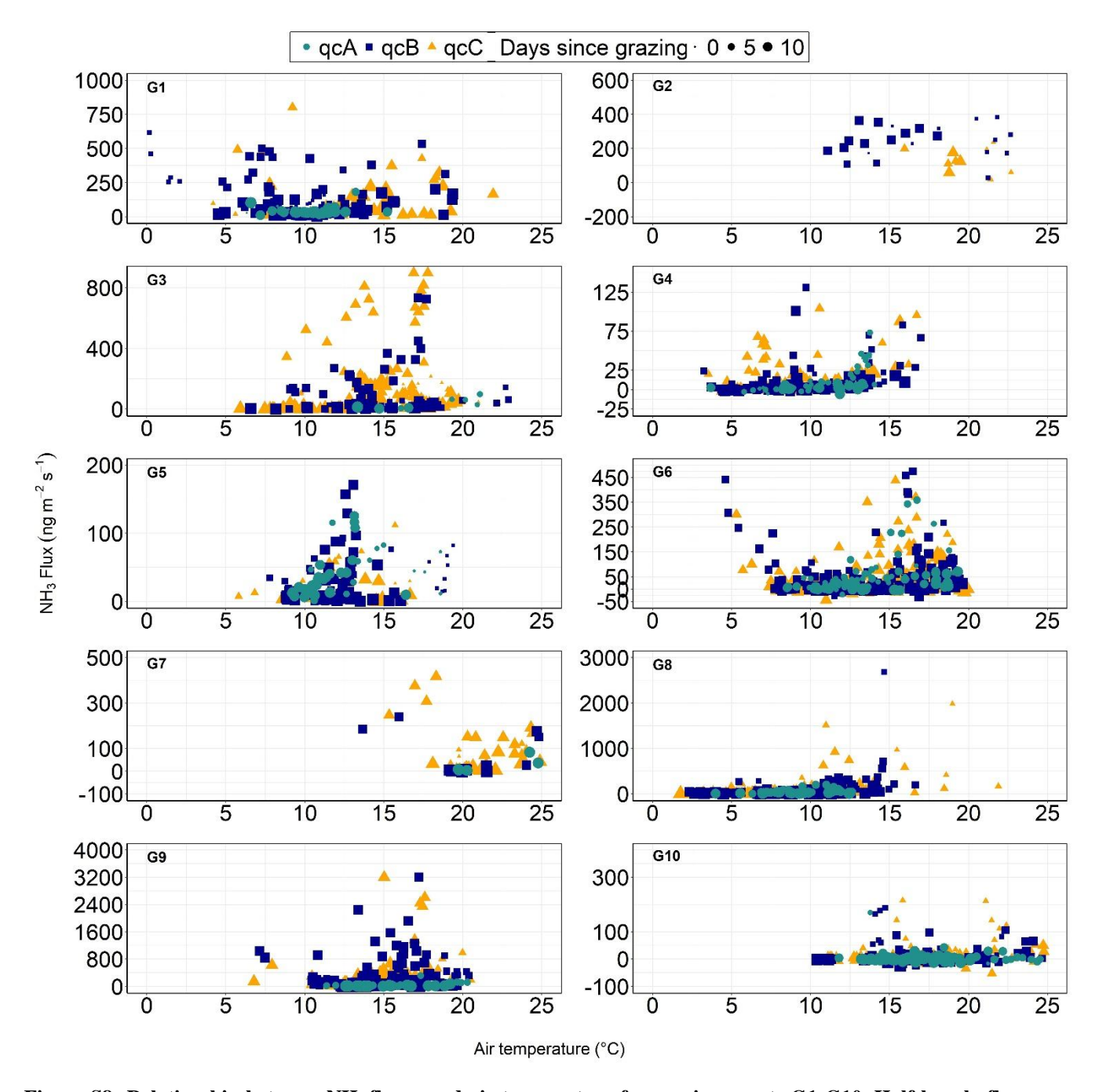


Figure S8: Relationship between NH₃ fluxes and air temperature for grazing events G1-G10. Half-hourly fluxes are shown. Symbol sizes correspond to the time elapsed since the grazing event started.

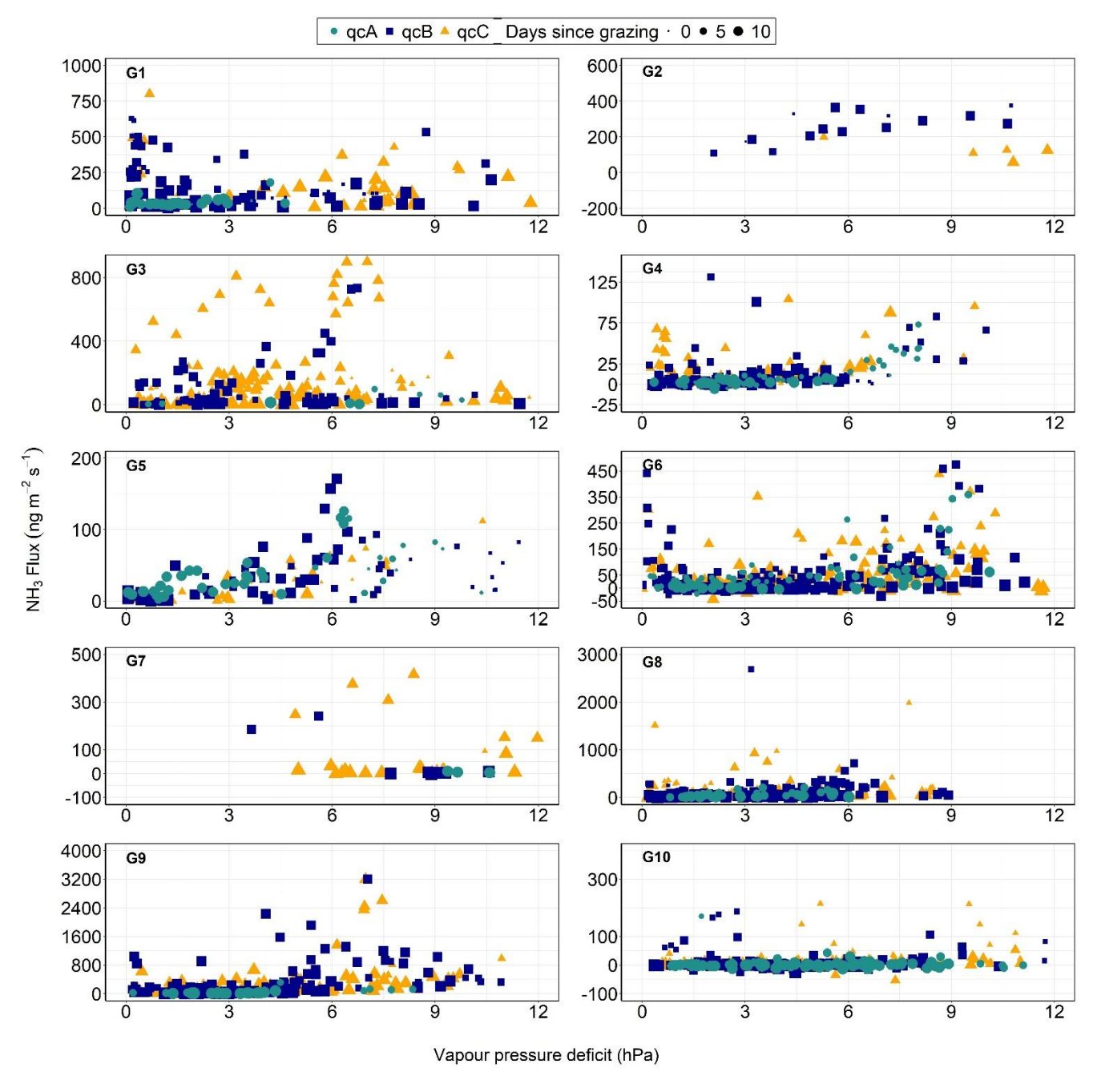


Figure S9: Relationship between NH₃ fluxes and VPD for grazing events G1-G10. Half-hourly fluxes are shown. Symbol sizes correspond to the time elapsed since the grazing event started.

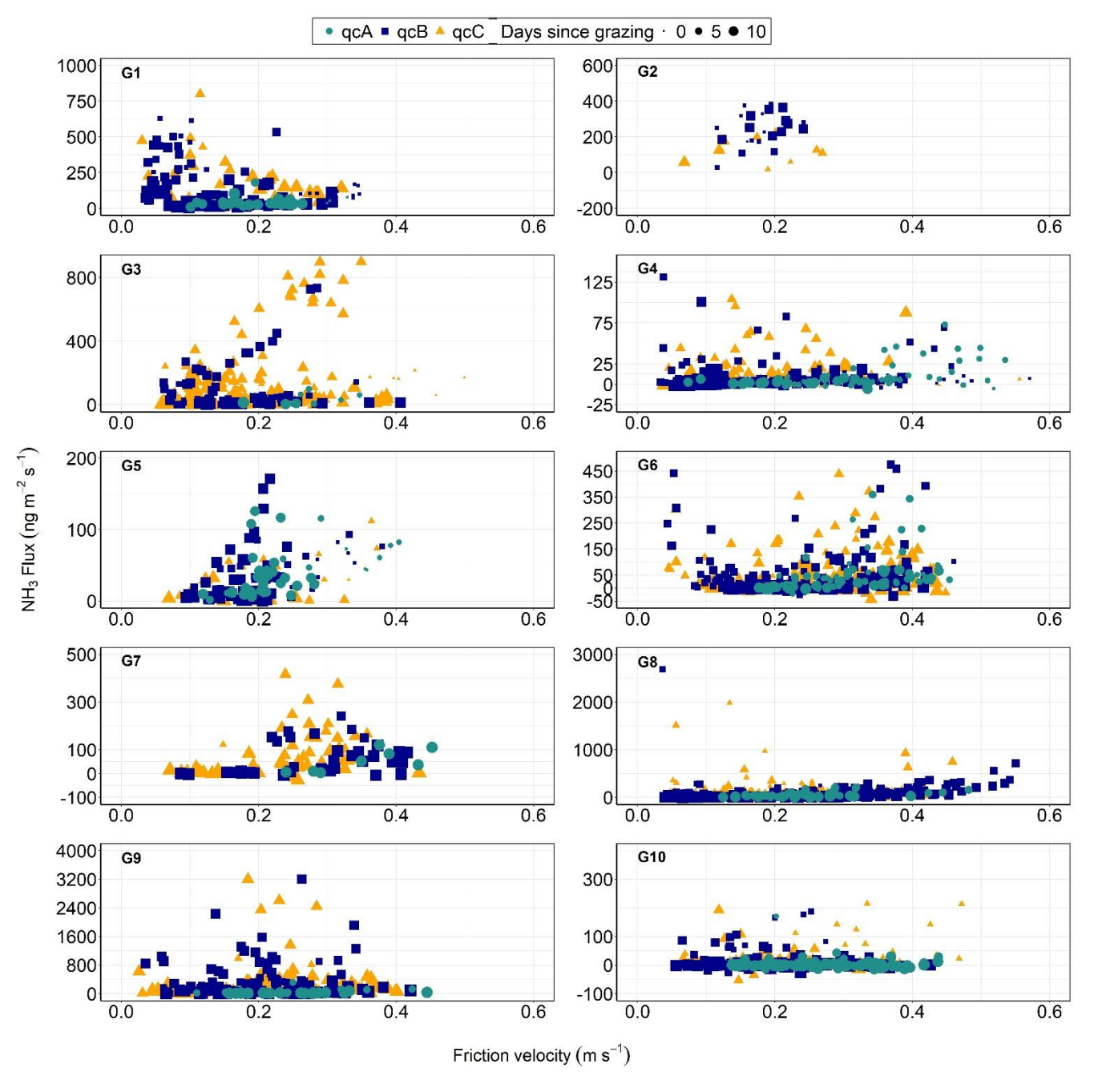


Figure S10: Relationship between NH₃ fluxes and friction velocity(u*) for grazing events G1-G10. Half-hourly fluxes are shown. Symbol sizes correspond to the time elapsed since the grazing event started.

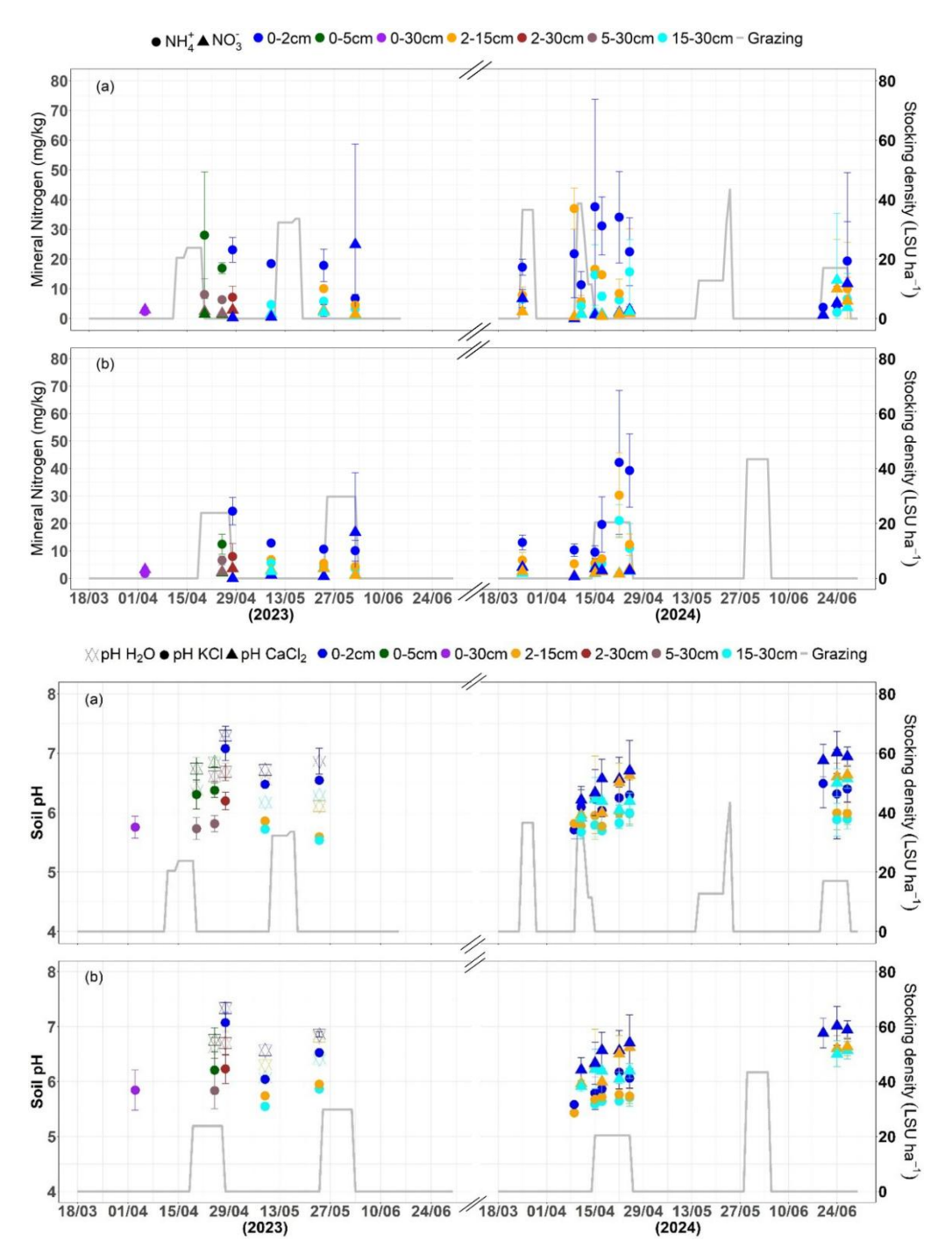


Figure S11: Top: Soil mineral nitrogen concentrations (NH_4^+ and NO_3^-) variation across different soil depths (0–30 cm) in relation to grazing activity in 2023 and 2024 for (a) Plot A and (b) Plot B; Bottom: Soil pH variation across different soil depths (0–30 cm) in relation to grazing activity in 2023 and 2024 for (a) Plot A and (b) Plot B. Error bars denote standard deviations across replicates.

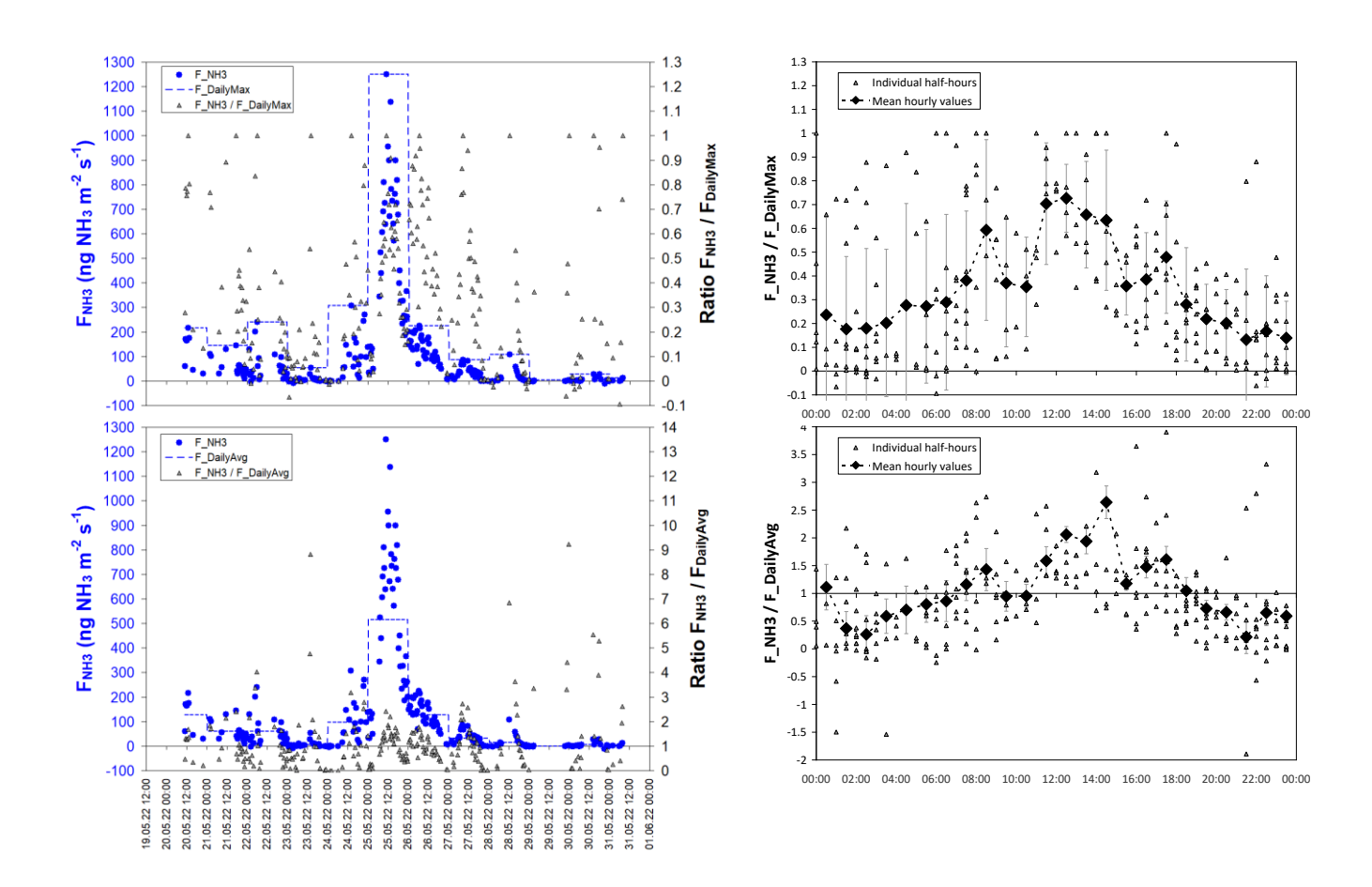


Figure S12: Example calculations for grazing period G3 of the mean diurnal flux patterns, with top: DVmax calculation method and bottom: DVavg method (see equations S5-S6 in Supplement S6).

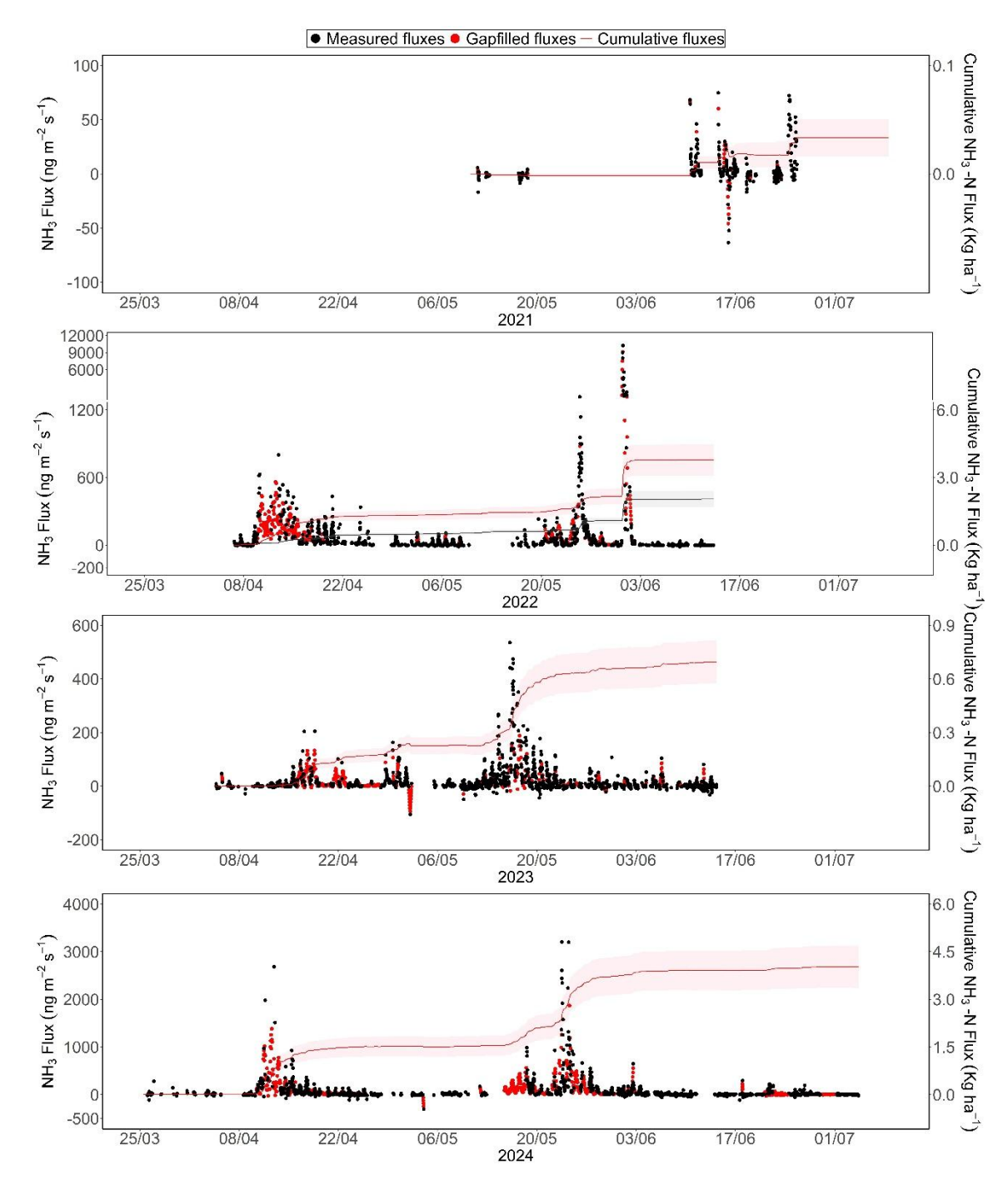


Figure S13: Measured (black) and gap-filled (red) NH₃ fluxes and cumulative emissions for 2021–2024 in Plot A. Gap-filling was performed using linear interpolation outside grazing periods and the DVmax method during grazing (see section 2.6 in the main text). The red lines indicate cumulative emissions over the season. Red-shaded areas indicate uncertainty in cumulative NH₃ flux estimates.

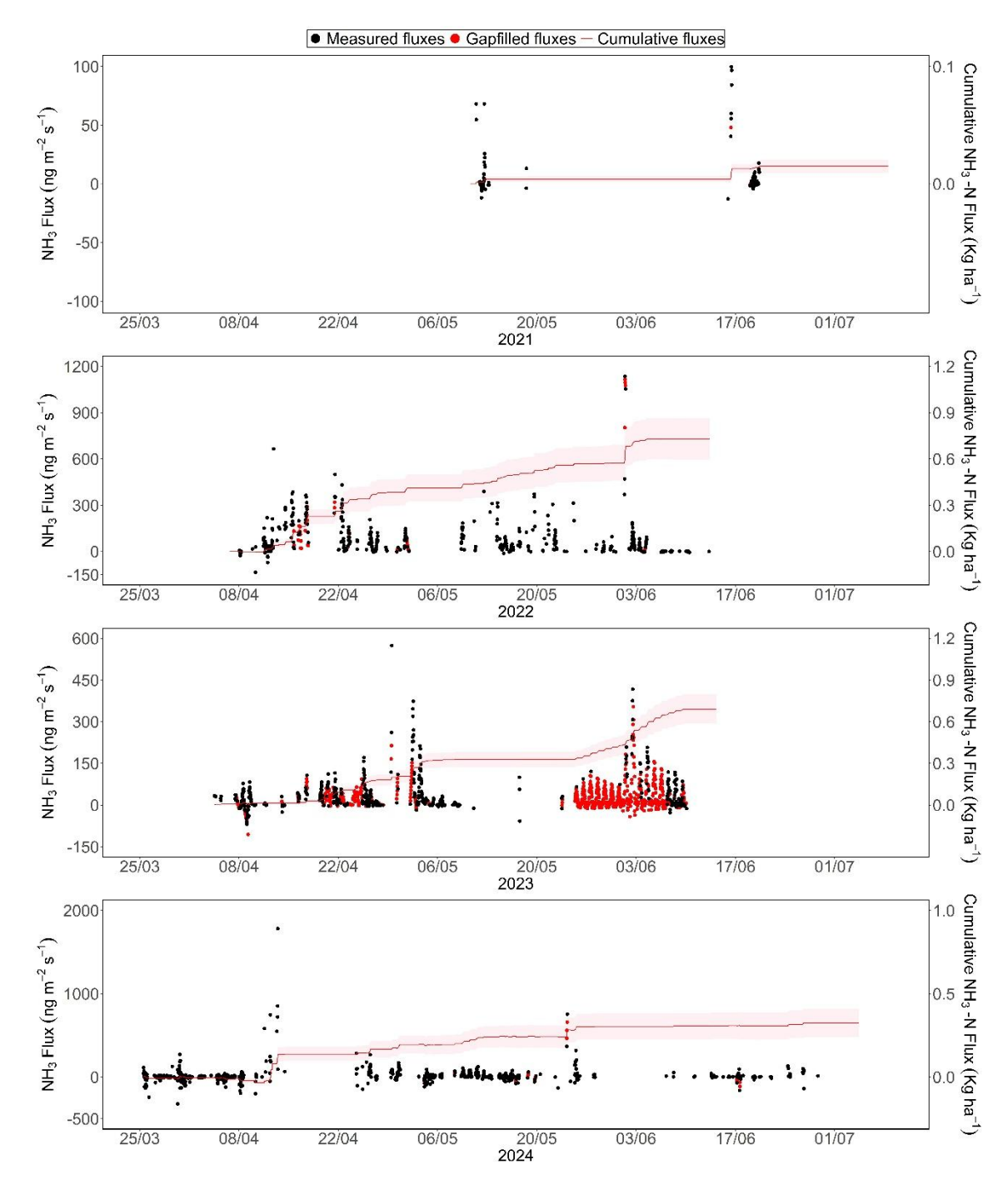


Figure S14: Measured (black) and gap-filled (red) NH₃ fluxes and cumulative emissions for 2021–2024 in Plot B. Gap-filling was performed using linear interpolation outside grazing periods and the DVmax method during grazing (see section 2.6 in the main text). The red lines indicate cumulative emissions over the season. Red-shaded areas indicate uncertainty in cumulative NH₃ flux estimates.

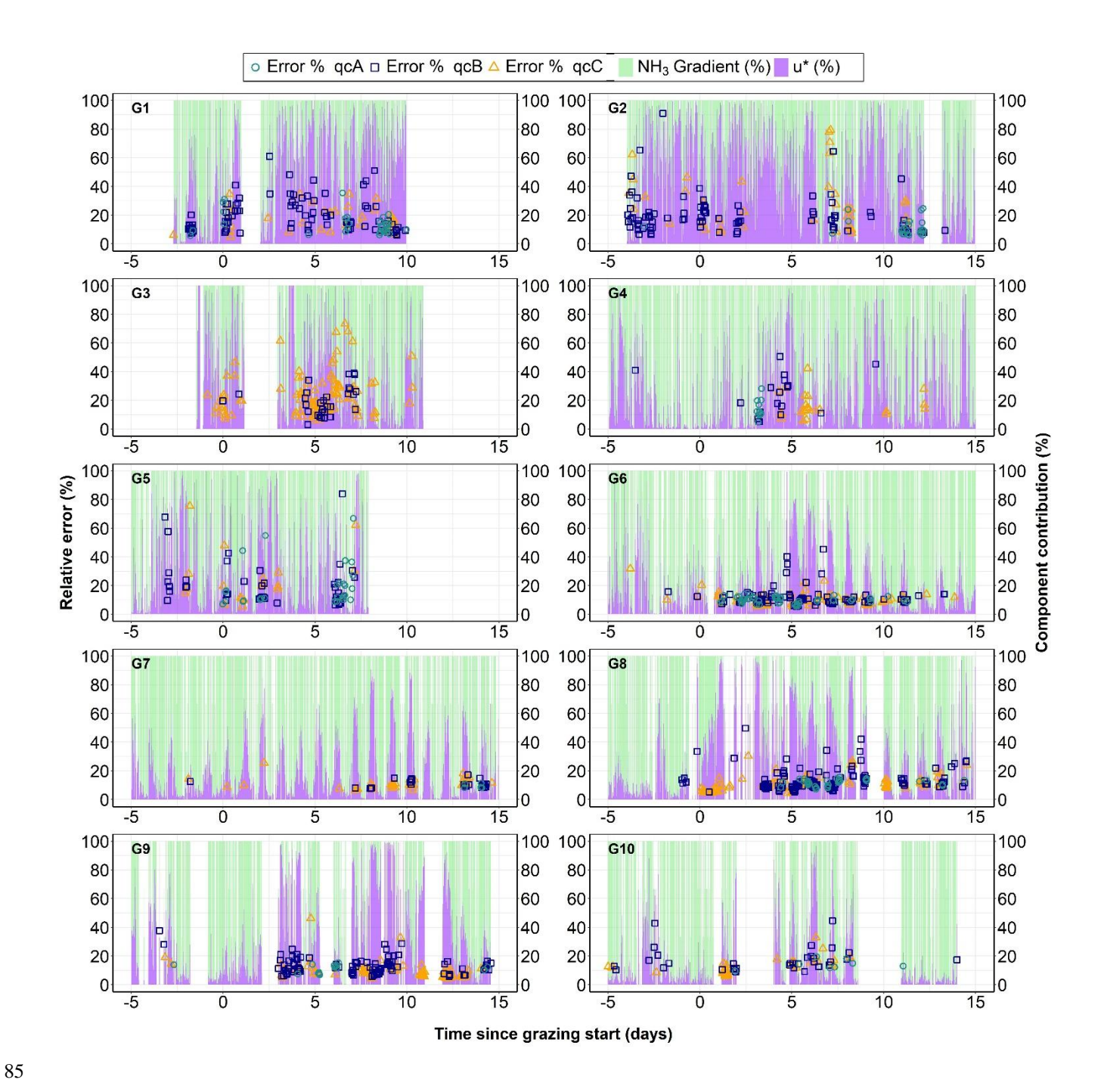


Figure S15: Relative random errors (%) in NH₃ flux measurements across grazing events G1–G10. Coloured markers represent flux quality classes: qcA (circles), qcB (squares), and qcC (triangles). The background shaded areas indicate the contributions of NH₃ concentration gradients (green) and friction velocity u* (purple) to overall flux uncertainty.

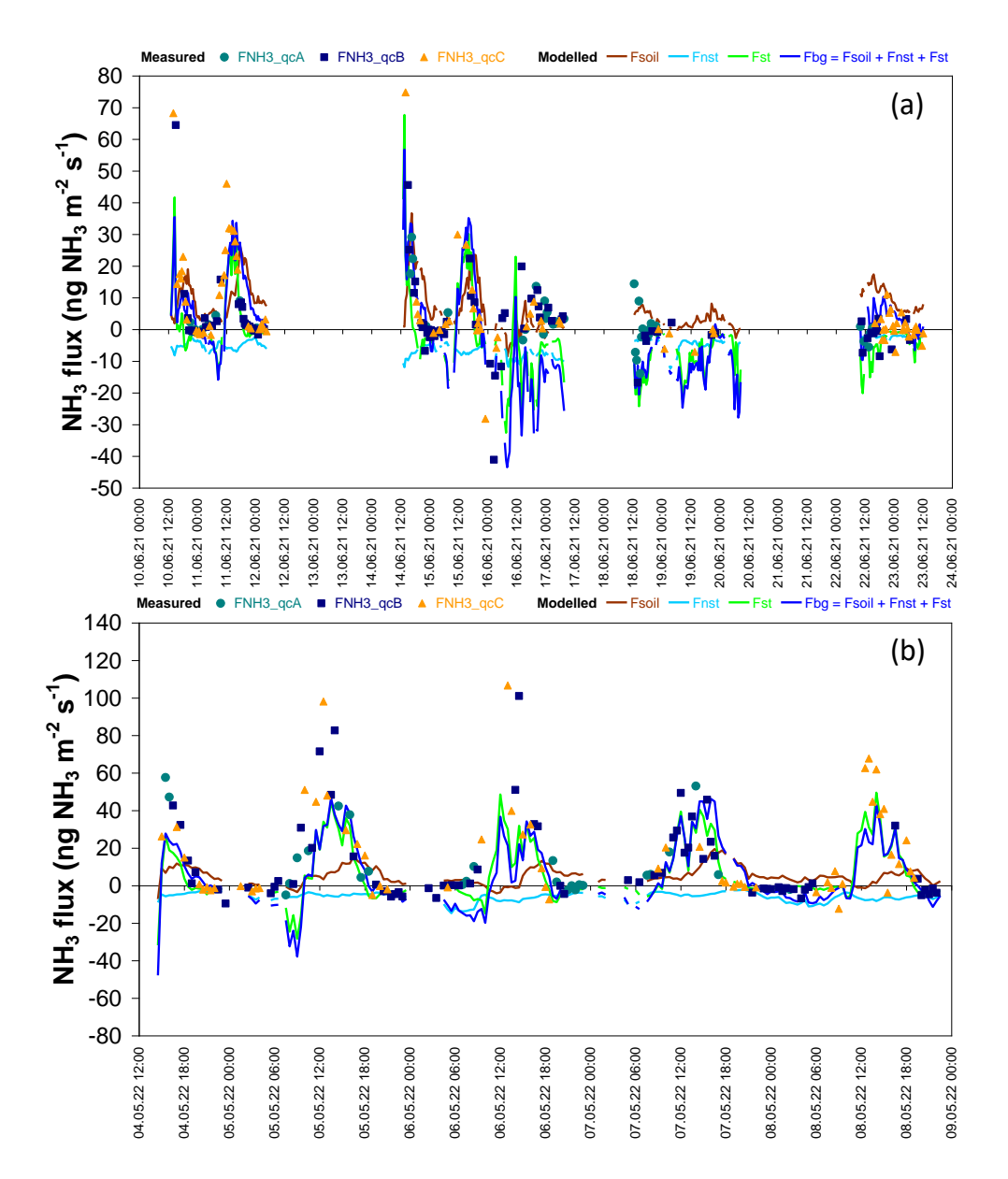


Figure S16: Example bi-directional NH₃ flux data measured in background conditions (well outside of grazing or fertilization periods) in springs 2021 (a) and 2022 (b), showing typical alternating diurnal patterns of NH₃ emissions and dry deposition. The bi-directional, 2-layer NH₃ canopy compensation point exchange model developed by Nemitz et al. (2001) and further refined by Massad et al. (2010) was applied to the data, simulating three component fluxes (soil flux F_{soil} , stomatal flux F_{st} and non-stomatal deposition flux F_{nst}) and the resulting net canopy-scale background flux F_{bg} as the sum of the three components. The model parameters Γ_{stomata} and Γ_{soil} (ratios of NH₄⁺ to H⁺ concentrations in leaf apoplast and soil water-filled pore space, respectively) were adjusted to fit the measured fluxes for each year, with Γ_{stomata} values of 800 and 1800 in 2021 and 2022, and Γ_{soil} values of 2000 and 3000 in 2021 and 2022, respectively. The minimum resistance to non-stomatal deposition ($R_{w, min}$) was set to 50 s m⁻¹. See Nemitz et al. (2001) and Massad et al. (2010) for details.

Table S1: Meteorological and ecosystem data

Variables (units)	Measurement system (supplier)	Acquisition frequency (averaging)	Comments
Micro/Meteorology			
Wind speed and turbulence u, v, w, SOS (m s ⁻¹), T (C)	3-D ultrasonic anemometer (HS-50, Gill Instruments Ltd., UK)	20 Hz (30 min)	2 m above ground
Friction velocity u*, (m s ⁻¹) Sensible heat flux H, (W m ⁻²) Obukhov length L, (m)	Eddypro software (v 7.0.9, LI-COR Biosciences, Lincoln, NE, USA)	30 min intervals	Eddy covariance post- processing
Rainfall (mm)	Tipping bucket rain gauge (ARG314, Campbell Scientific, USA)	1 min (30min)	0.1 mm resolution
Air temperature (C) Relative humidity (%) Vapour pressure deficit VPD (hPa)	Thermo-hygrometer (HMP155 Humicap probe, Vaisala GmbH, Germany)	30 sec (30min)	2 m above ground
Global (R _g) and net (R _n) radiation	Net radiometer (CNR4, Kipp and Zonen, NL)	20 sec (30min)	
Soil temperature	Thermocouples (T109, Campbell Scientific, USA)	1 min (30min)	Soil depths 5, 15, 35, 50 cm
Soil water content Time domain reflectometry prob (CS650, Campbell Scientific, U		1 min (30min)	Soil depths 5, 15, 35, 50 cm
Ecosystem-related variables			
Above-ground biomass	Strip mower	Day before every grazing event	Strips of 0.5*6 m (3 m ²), 3 reps per field
Canopy height	Herbometer	Day before and after every grazing event	100 reps per field
Leaf area index	Sunscan probe (model SS1) and BF5 sunshine sensor (DELTA-T Devices Ltd, UK)	Day before every grazing event	20 reps per field
Bulk N content of vegetation	k N content of vegetation Total C/N elemental analyzer (Flash EA 1112 Series, Thermo Finnigan, USA)		Uses samples from strip mower
Soil pH and mineral nitrogen	See Supplement section S5	See Supplement Fig. S11	

Table S2: Micrometeorological screening components (% valid) of data meeting quality criteria (0 or 1) and contribution of the random error components

	Percentage of 0 and 1 data (%)				Random error contribution (%)		
Period	qcH	qcL	qc_{τ}	qс _{NH3} stationarity	$qc_{\mu met}$	u*	χ*
G1	93.3	79.6	95.6	88.8	62.2	58.4	41.6
G2	95.3	82.9	97.4	100.0	78.8	63.9	36.1
G3	96.0	87.6	98.1	99.8	83.4	32.1	67.9
G4	96.5	87.9	98.2	97.1	81.5	20.4	79.6
G5	96.3	88.2	98.1	97.9	81.9	29.2	70.8
G6	97.0	92.8	97.7	94.0	84.7	24.3	75.7
G7	96.4	94.6	99.0	93.4	84.6	41.8	58.2
G8	93.5	84.7	96.5	88.9	69.3	41.6	58.4
G9	95.6	85.7	97.5	79.4	66.8	54.1	45.9
G10	93.0	85.4	97.2	64.9	55.1	17.3	82.7

Table S3: Pearson correlation coefficients between normalized half-hourly NH₃ fluxes (scaled by daily maximum) and key environmental variables for each grazing event. Statistically significant correlations are indicated as follows: ***p < 0.001, **p < 0.01, *p < 0.05; no symbol indicates $*p \ge 0.05$ (not significant). Air T refers to air temperature; Soil T, soil temperature; WS, windspeed; *u*, friction velocity; RH, relative humidity and VPD, vapour pressure deficit.

	Air T	Soil T	WS	u*	RH	VPD	Rainfall
Period	(°C)	(°C)	(ms^{-1})	(ms^{-1})	(%)	(hPa)	(mm)
G1	-0.01	-0.19*	-0.34***	-0.18*	-0.07	0.14	-0.08
G2	-0.21	-0.37*	0.23	0.35*	0.10	-0.20	-0.15
G3	0.34***	0.10	0.25***	0.23***	-0.31***	0.33***	-0.17**
G4	0.47***	0.37***	0.31***	0.32***	-0.50***	0.52***	-0.01
G5	0.15	0.11	0.10	0.27***	-0.26***	0.28***	0.14
G6	0.35***	0.20***	0.26***	0.29***	-0.32***	0.38***	-0.03
G7	0.21*	0.11	0.48***	0.49***	-0.39***	0.31***	-0.14
G8	0.31***	0.20***	0.38***	0.38***	-0.24***	0.27***	-0.05
G9	0.50***	0.31***	0.47***	0.46***	-0.44***	0.50***	-0.13*
G10	0.14*	0.19***	-0.07	-0.05	-0.21***	0.21***	0.04

Table S4: Pearson correlation coefficients between individual half-hourly NH₃ fluxes (actual) and key environmental variables for each grazing event. Statistically significant correlations are indicated as follows: ***p < 0.001, **p < 0.01, p < 0.05; no symbol indicates p ≥ 0.05 (not significant).

	Air T	Soil T	WS	u*	RH	VPD	Rainfall
Period	(°C)	(°C)	(ms^{-1})	(ms^{-1})	(%)	(hPa)	(mm)
G1	-0.20*	-0.36***	-0.48***	-0.34***	0.11	-0.04	-0.06
G2	-0.11	-0.30	0.13	0.22	-0.04	-0.07	-0.18
G3	0.18**	-0.03	0.53***	0.30***	-0.17**	0.16**	-0.11
G4	0.25***	0.21***	-0.03	0.01	-0.25***	0.32***	-0.05
G5	0.22**	0.30***	0.13	0.39***	-0.64***	0.59***	-0.17*
G6	0.18***	0.03	0.12**	0.15**	-0.32***	0.34***	-0.04
G7	-0.07	-0.01	0.34***	0.34***	-0.18	0.08	-0.10
G8	0.37***	0.27***	0.18***	0.13*	-0.03	0.13*	-0.04
G9	0.17**	0.14*	-0.06	0.00	-0.37***	0.36***	-0.10
G10	0.20***	0.16**	0.09	0.07	-0.21***	0.27***	-0.03

S1 DELTA Dry Denuder Sampling for Ammonia Concentration Reference

135

140

145

150

To provide a reference and correction for NH₃ concentration measurements made by the QCL instrument, we used UKCEH **DELTA®** denuder (DEnuder for Long-Term Atmospheric measurements sampling; https://www.ceh.ac.uk/solutions/equipment/air-sampler-systems-environmental-monitoring). The DELTA® system is a lowcost diffusion-based dry denuder, originally designed for long-term NH₃ sampling (Sutton et al., 2001). It operates on the principle of a single-bore glass denuder for sampling trace gases (Ferm, 1979), where a laminar air stream passes through the denuder coated on the inside with an acid solution (e.g., citric acid). The acid walls capture gas-phase NH3 to be later extracted in the laboratory, while slower-diffusing, NH₄⁺ -containing aerosols pass through and are collected by aerosol filters placed downstream of the denuder. Air is drawn through the denuder at 0.3-0.4 l min⁻¹, ensuring very efficient NH₃ scrubbing while allowing aerosols separation.

In this study, DELTA® denuders were deployed in the field at a height of 1.1 m, co-located and aligned with the mid-point of the NH₃ gradient mast. After exposure, the denuders were analysed for ammonium (NH₄⁺) content using continuous flow analysis (CFA) and spectrometric detection following ISO 11732:2005. With a near-100% capture efficiency for gas-phase NH₃ and a high-precision total (time-integrated) flow measurement, the DELTA® system is expected to yield a near-absolute mean NH₃ concentration over an exposure period. The DELTA® system was originally tuned for long-term concentration monitoring, with typically monthly sample change-over frequency, but shorter and longer periods are also possible, depending on ambient concentrations. Here, we used much shorter exposure intervals of typically 1-3 days during grazing and fertilization events and 1-2 weeks during background phases to increase the number of comparison points with the QCL instrument. These DELTA® NH₃ concentration data were then used to correct a posteriori the whole LGR-FTAA NH₃ concentration dataset, using linear regressions of the DELTA® data points versus the mean LGR-FTAA concentrations computed for each of the DELTA® sampling intervals (see Fig. 2 in main article).

S2 QCL NH₃ concentration gradient detrending procedure

170

175

180

To account for potential biases in vertical gradients arising from sequential sampling (non-simultaneous concentration measurements at the different heights) and non-stationary conditions, the OCL NH₃ concentration gradient data were 155 detrended, and the final half-hourly concentrations were calculated, using the following procedure.

- 1- The 10-second average concentrations NH₃(z, i) are calculated for each of the N sampling heights (z), for each of the nine 200-sec lift ascent cycles (i=1..9) of each half-hour (as shown in Fig. S1, see above)
- 2- For all nine cycles of each half-hour, at each height (z) of the N-point gradient, a trend (slope) is calculated between 160 cycle (i) and cycle (i+1) as follows:

slope(z, i, i+1) =
$$[NH_3(z, i+1) - NH_3(z, i)] / CycleDuration$$
 (S1)
with CycleDuration = 200 sec (slope unit : ppb s⁻¹).

- 165 3- A mean slope across all N sampling heights is calculated as follows: slope avg(i, i+1) = [slope(z1, i, i+1) + slope(z2, i, i+1) + ... + slope(zN, i, i+1)] / N(S2)
 - 4- The middle height (z=3 in a 5-point gradient, or z=2 in a 3-point gradient) is taken as the reference (zRef) and is not corrected. The other heights (z=1,2,4.5 in a 5-point gradient; or z=1,3 in a 3-point gradient) are corrected as follows: NH₃ corr(z, i) = NH₃(z, i) + slope avg(i, i+1) * Δt

(S3)

with Δt being the time interval (in seconds) between the end of height z (when the 10-sec concentration is calculated) and the end of the reference (middle) height (zRef). Δt is positive (negative) if height z is sampled before (after) zRef. Thus, for example, if there is an increasing trend over the interval of cycle (i) to (i+1), the heights sampled first (before zRef) are corrected upwards, and the heights sampled last (after zRef) are corrected downwards.

5- The half-hourly concentrations are calculated at each height as the average of the nine corrected concentrations within the half-hour:

$$NH_3 = 30min(z) = [NH_3 = corr(z, 1) + NH_3 = corr(z, 2) + ... + NH_3 = corr(z, 9)] / 9$$
 (S4)

S3 Response time constants of the QCL sampling system

185

190

195

The combined inlet-spectrometer-pump sampling system has a relatively rapid response time, adequate for profile sampling (though not fast enough for eddy covariance), which reflects intrinsic analyser response time, internal volume turnover and tube/cell wall damping effects. Characteristic response times $\tau 1$ and $\tau 2$ for the measurement system were obtained by fitting double exponential decay curves to concentration time series following a step change in NH₃ concentration (see e.g. Ellis et al., 2010). The fitted fast time constant $\tau 1$ was 1.4sec, corresponding to the sample gas turnover (pumping) rate in the internal volume. The slow time constant $\tau 2$ was 10 sec, which is function of the damping/smoothing effect of internal surfaces (tube and cell walls, filter surfaces). See Bell (PhD thesis, 2017) for details.

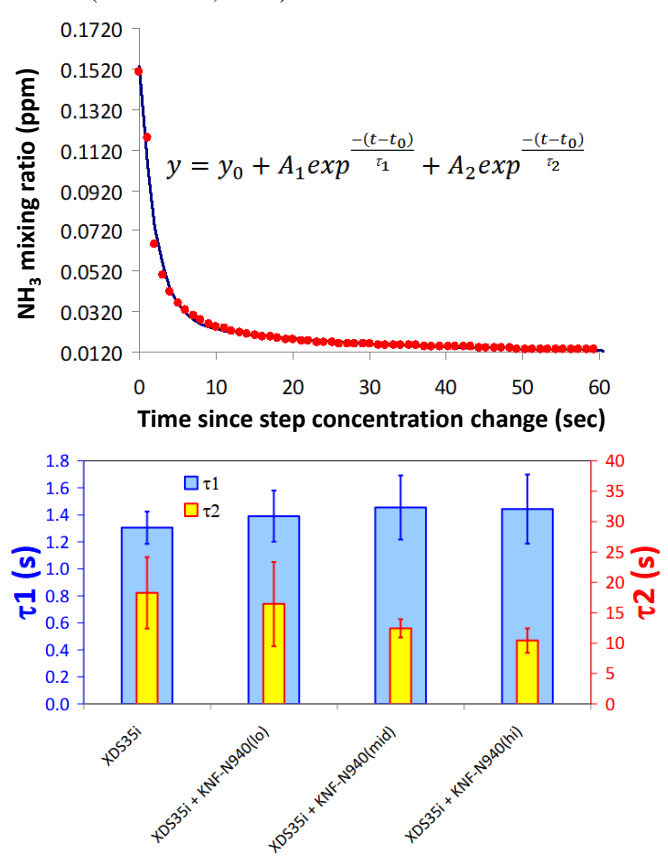


Fig. S17. Characterization of the fast $(\tau 1)$ and slow $(\tau 2)$ time constants of the LGR-FTAA-based NH₃ sampling system, obtained by fitting double exponential decay curves to concentration time series following a step change in NH₃ concentration (example time series shown in the top panel). The lower panel summarizes a series of decay experiments made using i) either the main Edwards XDS35i vacuum pump only, or ii) both Edwards XDS35i and the auxillary KNF-N940 pump, with the latter operating at low, intermediate and high flow rates. The auxillary KNF pump helps increasing the flow rate through the inlet line, from the aerosol cyclone to a T-piece at the back of the analyzer, thereby minimizing adsorption/desorption of NH₃ on tubing walls and thus decreasing the slow $\tau 2$ time constant to around 10 seconds.

S4 Momentum and sensible heat flux screening: the quality flagging system by Mauder and Foken (2004)

Momentum and sensible heat flux screening: the quality flagging system by Mauder and Foken (2004) was applied to EC fluxes of momentum (qc_τ) and sensible heat (qc_H), to ensure adequate quality of EC-derived friction velocity (u_*) and sensible heat flux (H) for the purpose of AGM flux calculations. Their 0-1-2 flagging policy is now a de facto standard in networks such as ICOS, AmeriFlux and FLUXNET. "0" means high-quality fluxes, "1" means fluxes are suitable for budget analysis, "2" means fluxes that should be discarded from the resulting dataset due to bad quality. The overall flag is determined as a combination of a steady state test (compares the statistical parameters determined for the averaging period and for short intervals within this period, with score 1-9), and an integral turbulence characteristics test (verifies whether the ratio of the standard deviation of a turbulent parameter to its turbulent flux is nearly constant or a function of stability, with score 1-9). Measurements flagged as 2 by the Eddypro® software (v7.0.9) were excluded while flags of 0 and 1 (combinations of qc_τ/qc_H 0/0, 0/1, 1/0, 1/1) were deemed acceptable and retained.

S5 Soil Sampling and Analysis for mineral Nitrogen and pH

200

205

210

215

220

Soil samples for the determination of nitrate (NO_3^--N) and ammonium (NH_4^+-N) were collected before and after grazing from 24 points in the sampled field during 2023 and 2024. Initially (early 2023), samples were taken from the top 0-30 cm soil layer. In subsequent campaigns, sampling was stratified into three depths: 0–2, 2–15, and 15–30 cm. Composite samples were made from these, resulting in four composite samples per depth. Samples were stored in polythene bags, labelled with indelible markers, placed in a cooler, and transported to the laboratory. On arrival, soil samples were sieved through a <2 mm mesh and frozen until analysis. Mineral nitrogen (NO_3^- and NH_4^+) was determined following NF ISO 14256-2 (March 2007). A 25 g portion of moist soil was extracted with 50 mL of 1 M KCl, agitated for 30 minutes, decanted and 20 ML of supernatant was then filtered through a 0.45 μ m syringe filter. The extracts were analyzed colorimetrically using a Smartchem 200 (AMS Alliance).

Soil pH was measured according to NF EN ISO 10390 (March 2022) on the <2 mm fraction using distilled deionized water 1 M KCl or 0.005 mol L⁻¹ CaCl₂ as extractants. The soil-to-solution ratio was 1:5 (10 g dry soil mixed with 50 mL of solution).

225 S6 Gap-filling approach and cumulative flux estimation for grazing event, based on mean diurnal variations

230

235

250

To estimate cumulative NH₃ emissions and grazing cattle EF, gaps in half-hourly time series of measured fluxes were filled using a statistical approach based on mean diurnal variations, in which mean diurnal cycles are calculated from the available flux data over several days of measurements, and missing fluxes at a certain time of day are assumed to equal the matching value from the mean diurnal cycle. A diurnal approach was necessary since flux patterns exhibited very strong differences between day and night (see Results).

However, this approach may lead to biased results if few flux data are available at certain times of the day, or especially at night when low wind speed and suppressed turbulence often lead to flux data rejection, and if outliers bias the calculated arithmetic mean of a small population. In addition, the very strong day-to-day dynamics in mean daily fluxes, and short-lived but very large peaks within a single grazing event, can also lead to biased mean diurnal cycles calculated over the whole grazing period. To reduce the risk of large biases associated with such temporal features, mean diurnal flux patterns were calculated in two stages:

1- Each corrected flux for the grazed plot (F_g) at hour "H" on day "D" was divided by (normalized to) the maximum flux of that day:

$$F'(H,D) = \frac{F_g(H,D)}{F_{dailyMax}(D)}$$
 (S5)

2- A mean diurnal cycle of the normalized dimensionless fluxes (F') was calculated from all available data over the grazing period. The normalized mean diurnal profile of F'_{avg}(H) thus varied between ~0 and 1.

The gap-filled flux (F_{gf}) for each missing flux value at hour H on day D was subsequently calculated as the product of the $F'_{avg}(H)$ value, looked up from the normalized mean diurnal cycle, by the maximum measured flux on day D:

$$F_{gf}(H,D) = F'_{avg}(H) \times F_{dailyMax}(D)$$
 (S6)

This method is subsequently referred to as the mean diurnal variation normalized to the maximum (DVmax). A variant of the same method was also implemented, whereby the fluxes were normalized to the daily average flux (DVavg) instead of the daily maximum. A graphical illustration of the steps involved in the calculation method is provided in Figure S12.

For grazing events (e.g., G9 and G10), where flux data were missing on some days (due to the quality filtering), a modified gap-filling approach was applied to maintain consistency with the DVmax/DVavg framework. For the G9 grazing event, the normalized mean diurnal variation approach (DVmax or DVavg) described previously could not be applied directly due to the absence of valid flux data (following quality filtering) during the first three days following grazing (D_g , D_{g+1} , D_{g+2}). To address this, a modified approach was implemented to ensure robust gap-filling while retaining consistency with the DVmax or DVavg method.

We identified the last day with the highest number of valid flux measurements before grazing and used it as a guiding reference day (D_{ref}) . The daily maximum $(F_{dailyMax}(D))$ for the missing early days were estimated by interpolating between $F_{dailyMax}(D_{ref})$ and values from subsequent valid days (e.g., D_{g+3} , D_{g+4} and so on).

$$F_{dailyMax}(D_g, D_{g+1}, D_{g+2}) = Interpolated\{F_{dailyMax}(D_{ref}), F_{dailyMax}(D_{g+3}), \ldots\}$$
 (S7)

For events with such gaps (e.g., G10) but where the missing daily flux values were located in the middle of the grazing event. In this case, the daily statistics (eg., F_{dailyMax}) for the missing day were estimated by interpolating between the earlier and later valid days within the same grazing period.

A variant of the approach was also implemented using the daily average (DVavg) instead of the daily maximum. The resulting daily scaling factors were then applied using the same DVmax or DVavg framework described earlier.

S7 Urinary nitrogen excretion during grazing

Ammonia fluxes in grazing systems are strongly influenced by urinary N excretion, which varies in concentration, volume, and frequency based on N intake, diet composition, and water intake. Urinary N characteristics were determined by utilising an empirical calculator (UriNGraze; Edouard et al., 2024), based on a combination of tools and equations from previous work. Daily herbage intake was estimated using the HerbValo method (Delagarde et al., 2017, Wlodarski et al., 2024), considering pasture conditions, animal factors (body weight and milk production) and forage or concentrate supplementation. This enabled calculation of dietary N intake and diet crude protein (CP) content from both herbage and supplemental feeds (feed CP content = feed N content × 6.25). From the diet CP content, plasma urea N concentration was estimated using a regression derived from the CowNFlow database (Ferreira et al., 2021; Delagarde and Edouard, 2023):

$$Plasma\ Urea\ (mg\ N\ l^{-1}) = -19.7\ +\ 0.2365\ \times\ CP\ content\ in\ diet(g\ kg\ DM^{-1}) \tag{S8}$$
 (Regression statistics: N = 114, R² = 0.82, sd = 3.81)

Plasma urea concentration was then used to determine urinary N excretion (g N cow⁻¹ day⁻¹) using the following metamodel (based on the model presented in Rouillé et al., 2019; equation adapted from Edouard et al., unpublished, which combines linear and quadratic terms):

Urinary N excretion (g N $cow^{-1} day^{-1}$) = ...

 $+ 0.0196 \text{ MY} + 0.00063 \text{ MY}^2 \dots$

+ 0.0609 UREA + 0.000043 UREA² ...

+ 0.00021 CONC.MPc + 0.000044 CONC.MY -0.00027 CONC.UREA ...

- 0.00093 MPc.MY - 0.00012 MPc.UREA ...

$$-0.00014 \text{ MY.UREA}$$
 (S9)

where CONC is the concentrate proportion (%), MPc the milk protein content (g kg⁻¹), MY the milk yield (kg cow⁻¹ day⁻¹), and UREA the plasma urea concentration (mg N l⁻¹).

290 The total N excreted per hectare during a grazing event was computed from daily urinary N excretion and total grazing days:

$$N_{event}(kg\ N\ ha^{-1}) = \frac{\text{Urinary N excretion}\left(g\ N\ LSU^{-1}day^{-1}\right) \times EGD(LSU\ ha^{-1}day)}{1000} \tag{S10}$$

where effective grazing days (EGD) were calculated as (see main article):

$$EGD = Stocking Density (LSU ha-1) \times Grazing Duration (days)$$
(S11)

275

References

- Bell, M. (2017). Emission, dispersion and deposition of ammonia from the plot to the landscape scale. PhD thesis, Agrocampus Ouest, Université Européenne de Bretagne, Rennes, France, 285 pp.
- 300 Delagarde, R., Caillat, H., and Fortin, J.: HerbValo: a paddock-level method for estimating the amount of pasture grazed annually by livestock. Fourrages, 2017, 229, pp.55-61.
 - Delagarde, R., and Edouard, N.: Plasma urea and diet crude protein concentration relationship in grazing dairy cows, Annual Meeting of the European Federation of Animal Science, Lyon, France, 2023.
- Edouard, N., Abdulwahab, M.O., Delagarde, R., Fauvel, Y., Ferreira, M., Flechard, C., Graux, A.-I., Lissy, A.-S., Robin, P., Vergé, X.. EMIGRAZE Stratégies d'alimentation associant fourrages pâturés et conservés : atouts ou contraintes pour l'efficacité azotée et les émissions gazeuses en élevage laitier, 2024. Final project report. https://librairie.ademe.fr/air/7949-emigraze-strategies-d-alimentation-associant-fourrages-patures-et-conserves.html.
- 310 Ellis, R.A. et al., 2010. Characterizing a Quantum Cascade Tunable Infrared Laser Differential Absorption Spectrometer (QC-TILDAS) for measurements of atmospheric ammonia. Atmos Meas Tech, 3(2): 397-406.
- Ferm, M.: Method for determination of atmospheric ammonia, Atmos. Environ., 13, 1385–1393, https://doi.org/10.1016/0004-315 6981(79)90107-0, 1979.
 - Ferreira, M., Delagarde, R., & Edouard, N.: CowNflow: A dataset on nitrogen flows and balances in dairy cows fed maize forage or herbage-based diets. Data in Brief, 38, 107393, 2021.
- Mauder, M. and Foken, T.: Documentation and instruction manual of the Eddy Covariance software package TK2, Univ Bayreuth, Abt Mikrometeorol., 26–42, available at: https://epub.uni-bayreuth.de/884/1/ARBERG026.pdf (last access: 27 March 2025), 2004.
- Rouillé, B., Gelé, M., Brun-Lafleur, L., Dumercy, L., Durand, A., Edouard, N., Faverdin, P., Lorinquer, E., and Mathias, E.: L'urée du lait: un indicateur pour estimer les rejets azotés et piloter l'alimentation des vaches laitières. Final project report, 2019. https://librairie.ademe.fr/recherche-et-innovation/754-uree-du-lait-un-indicateur-pour-estimer-les-rejets-azotes-et-piloter-l-alimentation-des-vaches-laitieres.html.
- Sutton, M. A., Tang, Y. S., Miners, B., and Fowler, D.: A new diffusion denuder system for long-term, regional monitoring of atmospheric ammonia and ammonium. in: Air-Surface Exchange of Gases and Particles, edited by: Fowler, D., Pitcairn, C., and Erisman, J.-W., Springer Netherlands, 145–156, https://doi.org/10.1007/978-94-010-9026-1_15, 2001.
- Wlodarski, L., Delagarde, R., Pozo, C.A., Ribeiro, H.M.N., Temp, L.B., Moraes, M.L., Santos, M.G., and Kozloski, G.V.: Calculating herbage utilisation and intake by dairy cows under subtropical conditions using conventional field measurement techniques or the HerbValo method, Tropical Animal Health And Production, 56-1, https://doi.org/10.1007/s11250-023-03863-2, 2024.